

Online Research @ Cardiff

This is an Open Access document downloaded from ORCA, Cardiff University's institutional repository: <https://orca.cardiff.ac.uk/id/eprint/113821/>

This is the author's version of a work that was submitted to / accepted for publication.

Citation for final published version:

Craco, L., Freelon, B., Alafailakawi, A. M., Karki, B. and Leoni, S ORCID: <https://orcid.org/0000-0003-4078-1000> 2018. Site-selective electronic structure of pure and doped Ca₂ O₃ Fe₃ S₂. Physical Review B 98 (4) , -. 10.1103/PhysRevB.98.045130 file

Publishers page: <http://dx.doi.org/10.1103/PhysRevB.98.045130>
<<http://dx.doi.org/10.1103/PhysRevB.98.045130>>

Please note:

Changes made as a result of publishing processes such as copy-editing, formatting and page numbers may not be reflected in this version. For the definitive version of this publication, please refer to the published source. You are advised to consult the publisher's version if you wish to cite this paper.

This version is being made available in accordance with publisher policies.

See

<http://orca.cf.ac.uk/policies.html> for usage policies. Copyright and moral rights for publications made available in ORCA are retained by the copyright holders.



Site-selective electronic structure of pure and doped $\text{Ca}_2\text{O}_3\text{Fe}_3\text{S}_2$

L. Craco,^{1,2} B. Freelon,³ and S. Leoni⁴

¹*Instituto de Física, Universidade Federal de Mato Grosso, 78060-900, Cuiabá, MT, Brazil*

²*IFW Dresden, Institute for Solid State Research, P.O. Box 270116, D-01171 Dresden, Germany*

³*Department of Physics, Massachusetts Institute of Technology, Cambridge, Massachusetts, 02139, USA*

⁴*School of Chemistry, Cardiff University, Cardiff, CF10 3AT, UK*

(Dated: June 9, 2018)

Using density functional dynamical mean-field theory we investigate the site-selective electronic structure of $\text{Ca}_2\text{O}_3\text{Fe}_3\text{S}_2$. We confirm that the parent compound with two distinct iron sites is a multi-orbital Mott insulator similar to $\text{La}_2\text{O}_3\text{Fe}_2\text{S}_2$. Electron/hole doping, carrier localization is found to persist on the two active iron channels because the chemical potential lies in a gap structure with anisotropic and almost vanishing states near the Fermi energy. This emergent behavior stems from large electronic reconstruction caused by dynamical spectral weight transfer involving states with distinct d -shell occupancies and orbital character at low energies. We detail the implications of our microscopic analysis and discuss the underlying physics which will emerge in future experiments on $\text{Ca}_2\text{O}_3\text{Fe}_3\text{S}_2$.

I. INTRODUCTION

In recent years the large family of Fe-based compounds^{1,2} has been the subject of intensive research after the discovery of high temperature superconductivity (high- T_c) in F-doped LaOFeAs .³ It has emerged that these unconventional superconductors (both pnictides and chalcogenides) increasingly fall into the bad-metal category. In $\text{SmFeAsO}_{1-x}\text{F}_x$,⁴ for example, suppression of superconductivity by high magnetic fields reveals a low temperature insulating behavior, similar to underdoped high- T_c cuprates.⁵ Interestingly, in some cases superconductivity arises directly from a normal state with insulating-like^{6,7} resistivity above T_c . Given telling similarities, along with notable differences, between the iron- and cuprate-based superconductors,⁸ an especially important issue has been to confirm whether the parent compounds are itinerant metals or if they lie in close proximity to a Mott metal-to-insulator transition.^{7,9} Particularly interesting for the latter view are Fe-oxychalcogenides, which have been synthesized with various compositions,^{2,10-14} showing different degrees of electron localization.

A Mott insulator undergoes an electronic phase transition to a correlated metal at low temperatures.¹⁵ The metallic behavior can vary from canonical Fermi to non-Fermi liquid depending on the degree of electronic correlation, disorder and structural-induced changes in orbital polarization patterns. In all cases, the insulator-to-metal phenomenon is due to the development of a severely renormalized lattice coherence scale, driven by increasing relevance of electronic delocalization upon external perturbations like pressure and chemical substitution.¹⁵ Optical and spectroscopic studies in 122-iron selenide superconductors,¹⁶ for example, show large-scale spectral weight transfer as function of temperature across the magnetic and superconducting phase instabilities, which is a fingerprint of Mottness.¹⁷

In this context, finding insulating and antiferromagnetically ordered ground state in layered Fe-

oxychalcogenides^{11,12,14,18,19} is relevant, since it confirms theoretical suggestions that Mott-insulating parent compounds in the Fe-superconducting systems could be found by increasing the ratio of the interaction-to-hopping beyond a critical value for a Mott transition.²⁰ The Fe-oxychalcogenides² thus help to sharpen the fundamental debate²¹ on the degree of electronic correlations in Fe-based superconductors in general. However, finding Mott electrons with different degrees of activation energies^{11-14,18} suggests strong multi-orbital (MO) electronic localization in this material class. In contrast to Fe-based superconductors, the consequences of Mottness (or the proximity to a insulator-metal transition) upon external perturbations in the Fe-oxychalcogenides has not received the theoretical attention it deserves. This is even more important, when the Mott transition is unconventional in nature, as shown here in $\text{Ca}_2\text{O}_3\text{Fe}_3\text{S}_2$ where carrier localization persists on different Fe-channels upon doping. Thus, following earlier studies on Fe-oxychalcogenides,^{22,23} we use the local density approximation plus dynamical mean-field theory (LDA+DMFT)²⁴ to study the role played by sizable MO electron-electron interactions in the Fe $3d$ shells of $\text{Ca}_2\text{O}_3\text{Fe}_3\text{S}_2$. As shown below, all five $3d$ -bands of two distinct Fe-sites (*Site 1*, *Site 2*) must be kept in order to satisfactorily resolve the site-selective Mott localization and bad metallic regimes obtained, respectively, for pure and doped $\text{Ca}_2\text{O}_3\text{Fe}_3\text{S}_2$. In MO Mott insulators, sizable electronic correlations drives new physical effects from (electron, hole) doping. They can induce a pseudogap regime, where the chemical potential lies in an energy region of vanishing density-of-states (DOS) near the Fermi energy (E_F),²⁵ or orbital-selective incoherent states, naturally yielding co-existent insulating and bad-metallic states as in cuprates²⁶ and Fe-pnictide superconductors.²⁷ In this work, we also use our results to discuss the influence of Mottness in lightly doped $\text{Ca}_2\text{O}_3\text{Fe}_3\text{S}_2$ providing specific predictions which can be tested in future experiments.

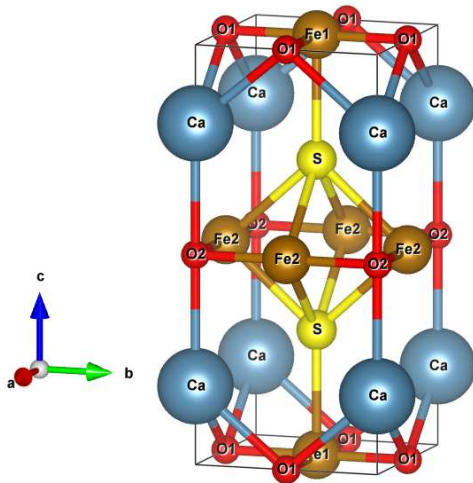


FIG. 1: (Color online) The three dimensional crystal structure of $\text{Ca}_2\text{O}_3\text{Fe}_3\text{S}_2$. Notice the two distinct iron sites.

II. RESULTS AND DISCUSSION

The crystal structure of $\text{Ca}_2\text{O}_3\text{Fe}_3\text{S}_2$ (space group $P4/mmm$) is built from alternate stacking of antiperovskite-like $[\text{Ca}_2\text{FeO}_2]^{2+}$ layers and $[\text{Fe}_2\text{OS}_2]^{2-}$ building blocks along the c -axis,¹³ as shown in Fig. 1. Similar to $\text{Na}_2\text{Fe}_2\text{OSe}_2$ oxychalcogenide Mott insulator,²² in the Fe_2OS_2 unit, the Fe^{2+} (d^6 electronic configuration) ions are located between oxygen atoms, forming a square-planar layer, which is an anti-configuration with respect to the CuO_2 layer of high- T_c cuprates. As seen in Fig. 1, the two-dimensional $[\text{CaFeO}_2]^{2+}$ layers contain FeO_2 planar sheets separated from the $[\text{Fe}_2\text{OS}_2]^{2-}$ layers by Ca ions. The Fe ions (*Site 2*) in the $[\text{Fe}_2\text{OS}_2]^{2-}$ blocks are sixfold-coordinated by two O ions and four S ions, forming a FeO_2S_4 octahedron. Extant refinement of structural data for the individual sites of $\text{Ca}_2\text{O}_3\text{Fe}_{2.6}\text{S}_2$ revealed that the Fe sites at the planar layer (*Site 1*) are fully occupied, while at *Site 2* the Fe ions are about 20% deficient in this vacancy ordered compound.

To explore the site-selective electronic structure of $\text{Ca}_2\text{O}_3\text{Fe}_3\text{S}_2$ parent compound, self-consistent band structure calculations were performed using the linear muffin-tin orbital (LMTO) method²⁹ in the atomic sphere approximation as implemented in PY LMTO computer code.³⁰ The Perdew-Wang parameterization³¹ was used to construct the exchange correlation potential within LDA. The total density was converged on a grid of 819 irreducible k points, and the radii of the atomic spheres were chosen as $r_{\text{Ca}}=3.57$ a.u., $r_{\text{O}}=1.97$ a.u., $r_{\text{Fe}}=2.45$ a.u., $r_{\text{S}}=3.12$ a.u. in order to minimize their overlap. The LDA calculation we performed using the cell parameter values reported elsewhere for $\text{Ca}_2\text{O}_3\text{Fe}_3\text{S}_2$ parent compound.¹³

Our results in Figs. 2 and 3 confirm that similar to

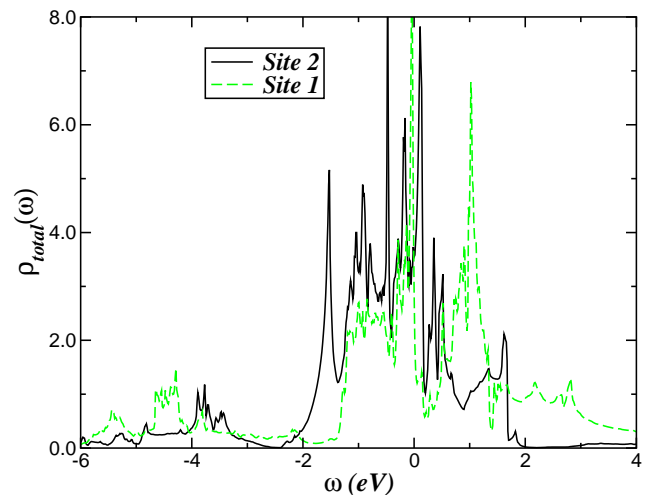


FIG. 2: (Color online) LDA site-resolved, total density-of-states (DOS) of paramagnetic $\text{Ca}_2\text{O}_3\text{Fe}_3\text{S}_2$. Notice the transfer of spectral weight from valence to conduction band at *Site 1* compared to *Site 2* due to changes in crystal fields on different layers, inducing an Fe^{3+} oxidation state at *Site 1*.

Fe-based superconductors the active electronic states involve Fe $3d$ carriers. A sizable enhancement of the average LDA bandwidth (W) relative to that of $\text{La}_2\text{O}_3\text{Fe}_2\text{S}_2$ ²³ due to short Fe-Fe bonds¹³ is obtained. As shown previously, $\text{La}_2\text{O}_3\text{Fe}_2\text{S}_2$ is a narrow band-gap Mott insulator,^{23,32} and the significantly larger on-particle bandwidth for $\text{Ca}_2\text{O}_3\text{Fe}_3\text{S}_2$ naturally implies proximity to metallization. Site- and orbital-driven anisotropies in the LDA band structure are also clearly manifested in Fig. 3. At *Site 2* the orbital-resolved DOS show similar features as found for $\text{La}_2\text{O}_3\text{Fe}_2\text{S}_2$, a result consistent with the Fe^{2+} oxidation state with six electrons in the Fe $3d$ shell. On the other hand, interesting deviations are seen for the xz, yz, xy and the $x^2 - y^2$ orbitals of *Site 1*, albeit less pronounced in the latter case. Due to changes in the crystal-field splittings the electronic states at *Site 1* are transferred to energies about E_F severely renormalizing the LDA orbital occupancies compared to *Site 2*, promoting a Fe^{3+} valence state (d^5 electronic configuration) with enhanced orbital polarization. Thus, we attempt to address the following question: How do electron correlations change from d^6 to d^5 electronic configuration? Typically going from partially to half-filled $3d$ electron shell electron correlation effects are expected to increase.³³ Here it is shown that this scenario holds true for $\text{Ca}_2\text{O}_3\text{Fe}_3\text{S}_2$. Additionally, as common to Fe-oxychalcogenides^{22,23} and peculiar to the Fe-based superconductors, strong crystal-field splitting effects lift the xz, yz orbitals degeneracy, leaving an antiferromagnetically ordered state at low temperatures¹³ without tetragonal-to-orthorhombic structural phase transition or orbital nematic instabilities. It thus follows that the novelties found in Fe-based superconductors,²⁸ relating to electronic nematic instabilities in

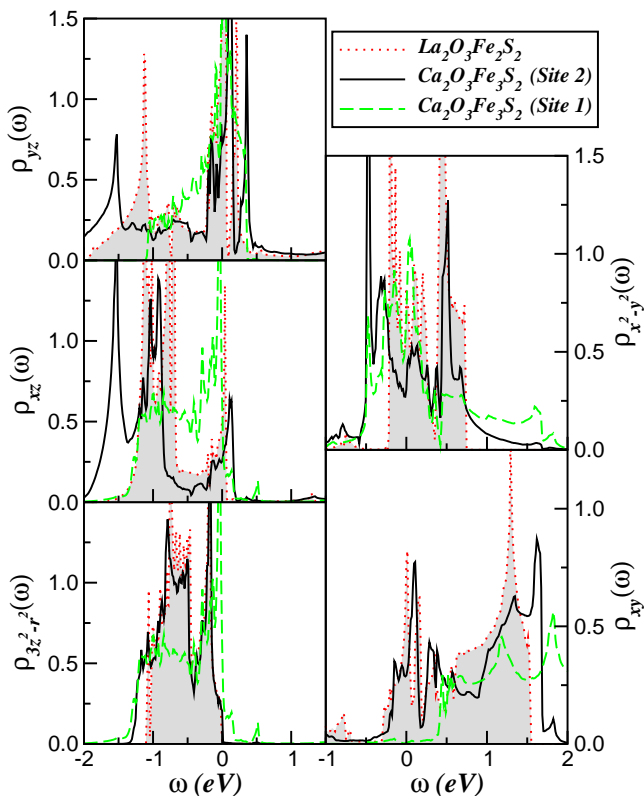


FIG. 3: (Color online) Site- and orbital-resolved LDA DOS for the Fe 3d orbitals of $\text{Ca}_2\text{O}_3\text{Fe}_3\text{S}_2$. Results for $\text{La}_2\text{O}_3\text{Fe}_2\text{S}_2$ parent compound are shown for comparison. Notice the site-selective nature of the electronic and the broad bands in the LDA DOS of $\text{Ca}_2\text{O}_3\text{Fe}_3\text{S}_2$ as compared to $\text{La}_2\text{O}_3\text{Fe}_2\text{S}_2$.

the tetragonal phase near the borderline of structural and magnetic transitions, will not play an active role in $\text{Ca}_2\text{O}_3\text{Fe}_3\text{S}_2$: Only spin nematic phase fluctuations³⁴ are expected to be seen across the magnetic phase transition of $\text{Ca}_2\text{O}_3\text{Fe}_3\text{S}_2$ at low temperatures.

Currently, the theoretical microscopic understanding of $\text{Ca}_2\text{O}_3\text{Fe}_3\text{S}_2$ is restricted to LDA and LDA+U calculations.¹³ Specifically, these *ab initio* density functional calculations demonstrate that the chalcogen and oxygen p states lie well below E_F and are weakly hybridized with Fe 3d states. Hence, the most relevant electronic states near the Fermi energy for $\text{Ca}_2\text{O}_3\text{Fe}_3\text{S}_2$ derive from the Fe layers with almost direct Fe-Fe hopping. In previous works we undertook systematic LDA+DMFT studies of Fe-oxychalcogenides, showing that narrow-band Kondo-Mott localization²³ and orbital-selective localization-delocalization transition²² can be understood within a single theoretical picture. Good semiquantitative agreement with experimental data of $\text{La}_2\text{O}_3\text{Fe}_2\text{M}_2$ ($M=\text{Se},\text{S}$) systems²³ serves as support to explore intrinsic, dynamical correlation effects in $\text{Ca}_2\text{O}_3\text{Fe}_3\text{S}_2$.

Although LDA+U provides reliable structural and magnetic ground state information of strongly correlated electron systems, it generically fails to capture

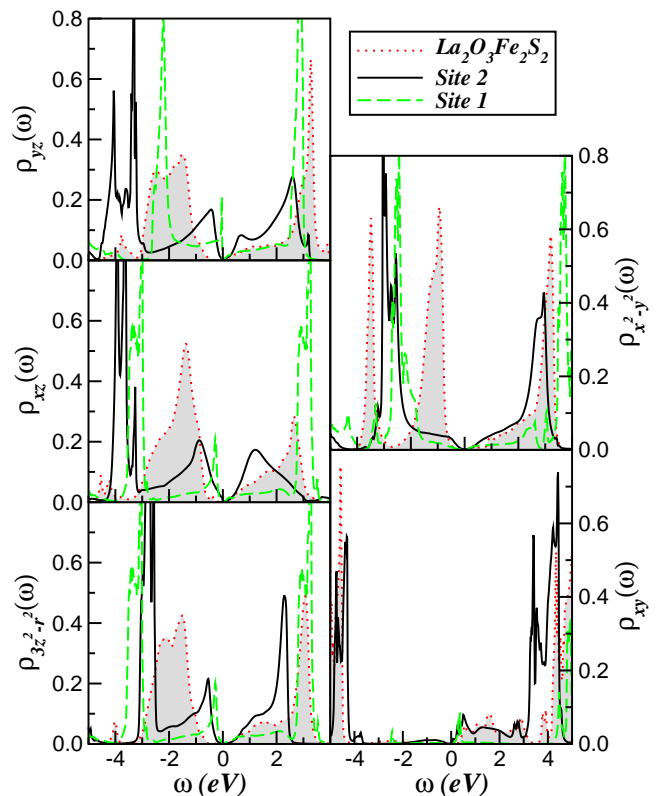


FIG. 4: (Color online) LDA+DMFT ($U = 5.0$ eV, $J_H = 0.7$ eV) spectral functions for the Fe 3d orbitals at *Sites 1* and *2* of $\text{Ca}_2\text{O}_3\text{Fe}_3\text{S}_2$. Notice the enhanced electronic localization at *Site 1* compared to *Site 2* as expected for half-filled correlated electron systems. Compared to LDA results, also worth noticing is the reduced orbital polarization due to sizable U' -induced inter-orbital-transfer of spectral weight.

the ubiquitous dynamical correlation effects in d -band compounds, and so cannot access normal state incoherence and the emergence of Hubbard satellites (local moments) at low and high energies. Combining LDA with DMFT is the state-of-the-art prescription for overcoming this problem.²⁴ Thus, as common to Fe-based superconducting materials³⁵ within LDA the one-electron part of the Hamiltonian for $\text{Ca}_2\text{O}_3\text{Fe}_3\text{S}_2$ reads $H_0 = \sum_{\mathbf{k},a,\sigma} \epsilon_a(\mathbf{k}) c_{\mathbf{k},a,\sigma}^\dagger c_{\mathbf{k},a,\sigma}$, where $a = 3z^2 - r^2, xz, yz, x^2 - y^2, yz$ label the (diagonalized in orbital basis) five Fe 3d bands, which are the only ones we retain, since the non-3d-orbital DOS at *Sites 1* and *2* have negligible or no weight at E_F .¹³ Here, the relevant inputs to our LDA+DMFT treatment for $\text{Ca}_2\text{O}_3\text{Fe}_3\text{S}_2$ are the LDA DOS for the five 3d orbitals at *Sites 1* and *2* shown in Fig. 3, the on-site Coulomb interaction U ,¹³ the inter-orbital term $U' = U - 2J_H$, and the Hund's coupling J_H . Based on this, at each Fe-channel the correlated part of the many-body Hamiltonian for $\text{Ca}_2\text{O}_3\text{Fe}_3\text{S}_2$ is $H_{int} = U \sum_{i,a} n_{i,a\uparrow} n_{i,a\downarrow} + \sum_{i,a \neq b} [U' n_{i,a} n_{i,b} - J_H \mathbf{S}_{i,a} \cdot \mathbf{S}_{i,b}]$. We choose values of $U = 5.0$ eV, $J_H = 0.7$ eV as employed in our earlier works for the Fe-oxychalcogenides.^{22,23} Our pa-

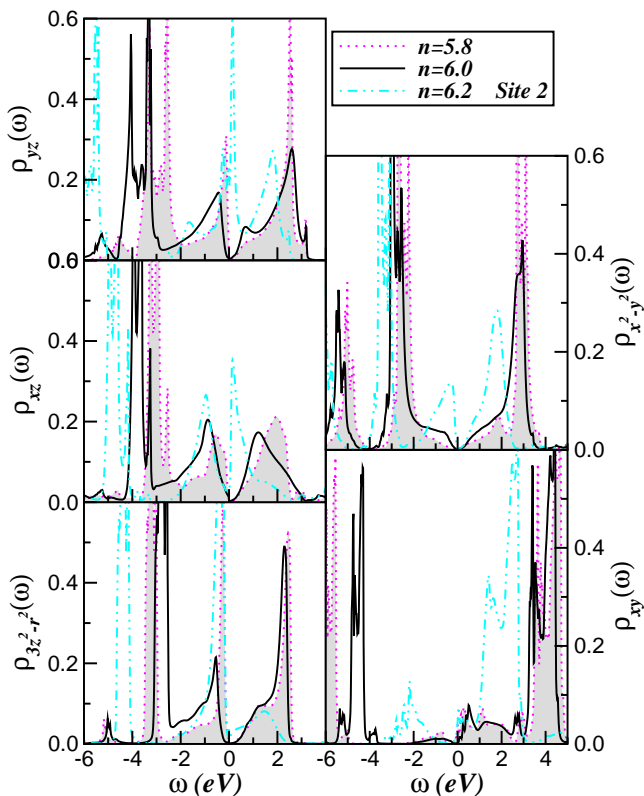


FIG. 5: (Color online) Effect of electron/hole doping on the LDA+DMFT ($U = 5.0$ eV, $J_H = 0.7$ eV) spectral functions for the Fe 3d orbitals of $\text{Ca}_2\text{O}_3\text{Fe}_3\text{S}_2$ at *Site 2*. Notice the electron delocalization and the appearance of incoherent, pseudogapped shoulders quasiparticle resonances on different orbitals near the Fermi energy.

parameter choice for the on-site Coulomb interaction is consistent with the U value used in Ref. 13 and the underlying view that Fe-oxychalcogenides are better regarded as strongly correlated electron systems.¹⁴ We evaluated the many-particle Green's functions of the Hamiltonian $H = H_0 + H_{int}$ above at *Sites 1* and *2* within LDA+DMFT,²⁴ using MO iterated perturbation theory (MO-IPT) as impurity solver.³⁶ The DMFT solution involves replacing the lattice model by a self-consistently embedded MO-Anderson impurity model, the self-consistency condition requiring the local impurity Green's function to be equal to the local Green's function for the lattice. The full set of equations for the MO case can be found in Ref. 36.

In the case of undoped $\text{Ca}_2\text{O}_3\text{Fe}_3\text{S}_2$, our LDA+DMFT results at both Fe-*Sites* (see Fig. 4) exhibit a Mott insulating gap in the orbital-resolved one-particle spectral functions. Several noteworthy features are observed: (i) Although rather small within the xy band, the Mott gap is orbital-dependent, i.e. intrinsically anisotropic. (ii) Carefully examining the orbital-resolved spectral functions of $\text{La}_2\text{O}_3\text{Fe}_2\text{S}_2$, one can see that the Mott phenomenon at *Sites 1* and *2* is weaker due to the presence of broad bands in $\text{Ca}_2\text{O}_3\text{Fe}_3\text{S}_2$ parent compound. As a result the

orbital-selective Mott gap is smaller due to reduced effective Coulomb repulsion, which is controlled by the intrinsic U/W ratio. Interestingly, (iii) our results at *Sites 1* and *2* display a behavior which suggest strong similarities with the Fe-oxychalcogenide systems.^{22,23} Namely, all orbitals are partially populated due to U' -induced dynamical inter-orbital entanglement.³⁶ As seen in Fig. 4, strong dynamical MO correlations originating from U, U' lead to sizable spectral weight redistribution over large energy scales and the formation of a severely reconstructed (compared to LDA) correlated electronic structure, with concomitant reduction of the orbital polarization patterns found in LDA. This behavior is characteristic of multiband Mott systems, where emergent upper and lower Hubbard bands are expected at high-energies. These latter features are known to be related to coupled spin-orbital local moments defining a Mott insulator without long-range charge, orbital or magnetic order.

Since there is no particle-hole symmetry in the bare electronic states of $\text{Ca}_2\text{O}_3\text{Fe}_3\text{S}_2$ (see Fig. 3), it is interesting to inquire what happens to the parent compound upon carrier (electron/hole) doping. In particular does selective localization characteristic of MO systems in the verge of Mott transition could be found in future studies on doped $\text{Ca}_2\text{O}_3\text{Fe}_3\text{S}_2$? Indeed, the generic appearance of incoherent metallic states with low energy pseudogaps, and the instabilities of such states to unconventional orders in a wide variety of correlated electron systems^{32,37} makes this an important question to inquire about. Our aim here is to build upon the strengths of MO correlated electronic structure calculations²⁴ to predict the effect of carrier doping on the two Fe-*sites* of $\text{Ca}_2\text{O}_3\text{Fe}_3\text{S}_2$. In particular we will discuss a set of predictions which could be tested in future experimental work.

Fig. 5 shows the changes in the correlated electronic structure upon electron and hole doping ($n \equiv 6 \pm \delta$) at *Site 2*. Similar to $\text{Na}_2\text{Fe}_2\text{OSe}_2$,²² when δ increases to small negative values a selective-Mott state develops, in which the $3z^2 - r^2, xz, yz$ and $x^2 - y^2$ spectral functions show behavior of a Mott insulator with vanishing DOS at E_F . While the xy orbital shows metallic behavior, characterized by the presence of incoherent in-gap states at E_F . On the other hand, enhanced metallicity is predicted for electron doped ($n = 6.2$) $\text{Ca}_2\text{O}_3\text{Fe}_3\text{S}_2$ where, in addition to the xy orbital, the xz, yz bands will also contribute to orbital-selective electronic transport and Fermi surface reconstruction within LDA+DMFT. Although the Mott gap in the $3z^2 - r^2$ and $x^2 - y^2$ band is considerably reduced upon electron doping, strong localization is clearly visible in this orbital sector, as seen in Fig. 5. From the above observation it can be suggested that strong Mottness²⁵ and orbital-selective Mott physics coexist in the Fe^{2+} electronic channel. Since there is no particle-hole symmetry in Fe^{3+} channel, it is interesting to inquire as to the effects of electron doping ($n \equiv 5 \pm \delta$) in this half-filled electronic reservoir. It is worth noticing here that electron-electron interactions are expected to reach their maximum at half-filling

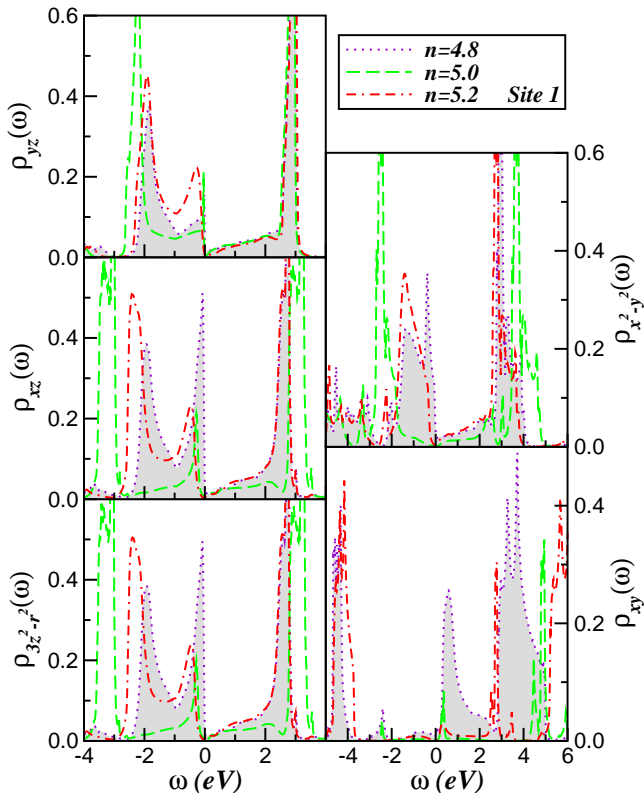


FIG. 6: (Color online) Effect of electron/hole doping on the LDA+DMFT ($U = 5.0$ eV, $J_H = 0.7$ eV) spectral functions for the Fe $3d$ orbitals of $\text{Ca}_2\text{O}_3\text{Fe}_3\text{S}_2$ at *Site 1*. A particular feature is the Mott delocalization upon electron doping of the parent compound and appearance of incoherent quasiparticle shoulders near the Fermi energy for $n = 4.8$. Selective Mott-localization and pseudogap features are the fingerprints of strong electronic correlations in multi-orbital systems close to half-filling.

and to decrease away from this configuration.³⁸ This expected electronic behavior is consistent with our results in Fig. 4 where strong correlation fingerprints are found at *Site 1* of $\text{Ca}_2\text{O}_3\text{Fe}_3\text{S}_2$ parent compound. Therefore, it is of fundamental importance to see if electron doping/hole is qualitatively different at *Site 1* compared to *Site 2* or, whether incoherent non-Fermi liquid behavior still emerges in the infrared region, or if Mott localization is favored. Fig. 6 exhibits the answer to this fundamental questions. As seen, Mott localization persists in all orbitals at *Site 1* for electron doped $\text{Ca}_2\text{O}_3\text{Fe}_3\text{S}_2$. On the other hand, metallicity is found to be favored upon hole doping, and the $x^2 - y^2, yz$ spectral functions show emergent spectral weight at E_F , while the $3z^2 - r^2, xz, yz$ spectral functions now show pseudogap behavior. Hence, hole doping *Site 1* of $\text{Ca}_2\text{O}_3\text{Fe}_3\text{S}_2$ is predicted to lead to orbital-selective metallicity compared to its electron doped counterpart.

What is the origin of these orbital-selective features? In a MO system like the Fe-oxychalcogenides, strong (in-

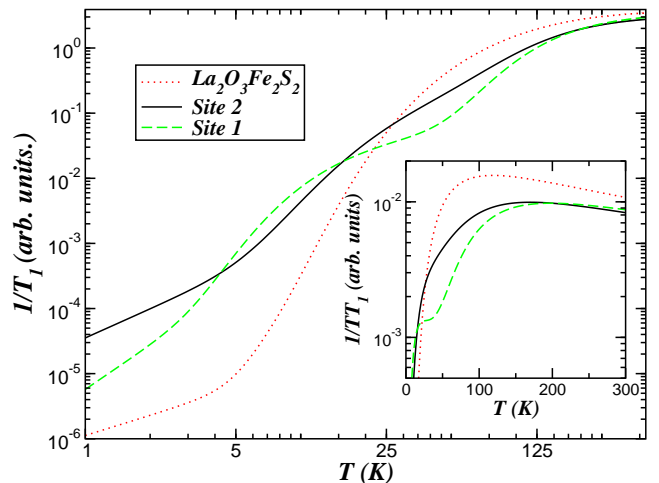


FIG. 7: (Color online) Channel-selective temperature dependence of spin-lattice relaxation rate ($1/T_1$) for $\text{Ca}_2\text{O}_3\text{Fe}_3\text{S}_2$ obtained with LDA+DMFT spectral functions (for $U = 5.0$ eV and $J_H = 0.7$ eV). The inset shows the corresponding nuclear spin relaxation rate ($1/T_1T$) results. Notice the similar power-law behavior within at both sites and the change in slope at low temperatures at *Site 2*, albeit less pronounced as compared to $\text{La}_2\text{O}_3\text{Fe}_2\text{S}_2$. This behavior marks the changes of multi-orbital spin fluctuation modes as T is reduced.

coherent) scattering between different carriers in orbital states split relative to each other due to the specific crystal field and one-electron band fillings leads to two main effects: (i) It leads, via static-Hartree contributions (from the static part of the orbital-dependent self-energies) to orbital-dependent shifts of the d -bands relative to each other, and (ii) strong dynamical correlations due to sizable U, U', J_H cause appreciable spectral weight transfer over large energy scales, from high to low-energy, upon carrier doping. This second feature leads to a drastic modification of the spectral lineshape as shown in Figs. 5 and 6. Microscopically, strong incoherent scattering, arising from co-existence of Mott-localized and bad metallic states, leads to an almost complete suppression of the Fermi liquid quasiparticles and the emergence of an incoherent spectra, reminiscent of what is seen in cuprate oxides. Our results imply that doped $\text{Ca}_2\text{O}_3\text{Fe}_3\text{S}_2$ should be located in pseudogap regime and the metallic state obtained by the filling-controlled Mott transition would be unconventional both at *Sites 1* and *2*. The origin of this emergent electronic state is the lattice orthogonality catastrophe³⁹ that occurs due to orbital-selective blocking of the coherent motion within LDA+DMFT due to sizable U' in the MO Hubbard model.

Armed with the above results, let us now discuss the implications of our results to future nuclear magnetic resonance (NMR) experiments. Here we recall that the spin-lattice relaxation rate ($1/T_1$) or the nuclear spin relaxation rate ($1/T_1T$) are directly computable using the DMFT propagators.^{40–42} While $1/T_1$ quantifies the

decay of the nuclear magnetic moments providing valuable information about the fluctuations of the electronic magnetic moments in the solid, $1/T_1T$ measures the slope of the imaginary part of the local spin susceptibility in the zero-frequency limit.⁴² With this caveat in mind, in Fig. 7 we display the temperature dependence of local dynamical spin fluctuations by computing the NMR spin-relaxation rate $1/T_1$ as a function of T within the paramagnetic phase of $\text{Ca}_2\text{O}_3\text{Fe}_3\text{S}_2$ as done earlier for the $\text{LaO}_{1-x}\text{FeAsF}_x$ system.⁴⁰ Though experimental data does not exist yet, the T -dependence of $1/T_1$ for $\text{Ca}_2\text{O}_3\text{Fe}_3\text{S}_2$ parent compound is predicted to show similar *Site*-dependent features in the non-magnetically ordered state of $\text{Ca}_2\text{O}_3\text{Fe}_3\text{S}_2$. By assuming the hyperfine coupling constants for the two Fe-sites to be identical, a particularly interesting feature to be seen is the power-law behavior and the change in slope at low temperatures, albeit less pronounced as compared to $\text{La}_2\text{O}_3\text{Fe}_2\text{S}_2$, which marks the changes of MO spin fluctuation modes as T is reduced. If the nuclear spin relaxation at both Fe sites is driven by a single spin degree of freedom, one would expect that the scaled relaxation rate be equal.⁴³ However, the different relaxation rates we obtain for $\text{Ca}_2\text{O}_3\text{Fe}_3\text{S}_2$ indicates that both the magnitude and the T -dependence of the two sites is not driven by the single relaxation mechanism, and that this relaxation mechanism is electronic state dependent. Enhanced Mott localization within Fe^{3+} electronic channel tends to suppress local spin fluctuations due to the formation of stronger localized moments in the half-filled shell. On the other hand the similarities in the relaxation rates seem to suggest that the Fe $3d$ spins fluctuate incoherently on both Fe *Sites*, so that both of them contribute to the relaxation almost similarly in future site-selective NMR experiments.

III. CONCLUSION

To summarize, we have used LDA+DMFT for a realistic two-channel Hubbard model with five active $3d$

bands at each channel to perform a detailed study of the paramagnetic Mott insulating state of $\text{Ca}_2\text{O}_3\text{Fe}_3\text{S}_2$. In particular, considering the Fe^{2+} ($S = 2$) and Fe^{3+} ($S = 5/2$) valence (spin) states intrinsic to this Fe-oxychalcogenide, we predict orbital-selective blocking of electrons and strong correlation fingerprints in the half-filled (Fe^{3+}) channel as an effect of multi-orbital Hubbard correlations. Compared to $\text{La}_2\text{O}_3\text{Fe}_2\text{S}_2$ short Fe-Fe bonds intrinsic to $\text{Ca}_2\text{O}_3\text{Fe}_3\text{S}_2$ lead to decreased electron correlation through increasing bandwidth, an undoubtedly significant feature also present in the high- T_c $\text{FeSe}/\text{SrTiO}_3$ system.⁴⁴ Interesting as well is the emergent electronic behavior when we consider the effect of electron/hole doping in this two-channel system. We predict that localization or low-energy incoherence persists in doped $\text{Ca}_2\text{O}_3\text{Fe}_3\text{S}_2$ due to a lattice orthogonality catastrophe induced by orbital-selective Mottness. This orbital blocking phenomenon can be directly tested by a combination of future spectral, transport and nuclear spin-lattice relaxation measurements. Such studies are called for, and should confirm or refute our predictions.

Acknowledgments

L.C.'s work is presently supported by CNPq (Grant. No. 304035/2017-3). S.L. acknowledges support from the UK Research Council for using work in the paper that was undertaken by a student under Project No. EP/M50631X/1 as well as the DFG for support under the priority project SPP1415 and for a personal Heisenberg grant. S.L. also thanks ZIH Dresden and ARCCA Cardiff for computational resources. Via S.L.'s membership of the UK's HPC Materials Chemistry Consortium, which is funded by EPSRC (No. EP/L000202), this work made use of the facilities of ARCHER, the UK's National High-Performance Computing Service, which is funded by the Office of Science and Technology through EPSRC's High End Computing Programme.

¹ D. C. Johnston, *Advances in Physics* **59**, 803 (2010); G. R. Stewart, *Rev. Mod. Phys.* **83**, 158 (2011); K. Deguchi, Y. Takano, and Y. Mizuguchi, *Sci. Technol. Adv. Mater.* **13**, 054303 (2012). For more recent overviews on iron based superconductors see also, M. K. Wu, P. M. Wu, Y. C. Wen, M. J. Wang, P. H. Lin, W. C. Lee, T. K. Chen, and C. C. Chang, *J. Phys. D: Appl. Phys.* **48**, 323001 (2015); Q. Si, R. Yu, and E. Abrahams, *Nat. Rev. Mater.* **1**, 16017 (2016).

² See also, C. Stock and E. E. McCabe, *J. Phys.: Condens. Matter* **28**, 453001 (2016) and references therein.

³ Y. Kamihara, T. Watanabe, M. Hirano, and H. Hosono, *J. Am. Chem. Soc.* **130**, 3296 (2008).

⁴ S. C. Riggs, J. B. Kemper, Y. Jo, Z. Stegen, L. Balicas, G.

S. Boebinger, F. F. Balakirev, A. Migliori, H. Chen, R. H. Liu, and X. H. Chen, *Phys. Rev. B* **79**, 212510 (2009).

⁵ R. W. Hill, C. Proust, L. Taillefer, P. Fournier, and R. L. Greene, *Nature (London)* **414**, 711 (2001); Y. Ando, S. Komiyama, K. Segawa, S. Ono, and Y. Kurita, *Phys. Rev. Lett.* **93**, 267001 (2004).

⁶ T. J. Liu, X. Ke, B. Qian, J. Hu, D. Fobes, E. K. Vehstedt, H. Pham, J. H. Yang, M. H. Fang, L. Spinu, P. Schiffer, Y. Liu, and Z. Q. Mao, *Phys. Rev. B* **80**, 174509 (2009); Y. Mizuguchi, F. Tomioka, S. Tsuda, T. Yamaguchi, and Y. Takano, *J. Phys. Soc. Jpn.* **78**, 074712 (2009); M. H. Fang, J. H. Yang, F. F. Balakirev, Y. Kohama, J. Singleton, and B. Qian, Z. Q. Mao, H.D. Wang, and H.Q. Yuan, *Phys. Rev. B* **81**, 020509 (2010).

- ⁷ T. Yamauchi, Y. Hirata, Y. Ueda, and Kenya Ohgushi, Phys. Rev. Lett. **115**, 246402 (2015); H. Takahashi, A. Sugimoto, Y. Nambu, T. Yamauchi, Y. Hirata, T. Kawakami, M. Avdeev, K. Matsubayashi, F. Du, C. Kawashima, H. Soeda, S. Nakano, Y. Uwatoko, Y. Ueda, T. J. Sato, and K. Ohgushi, Nature Materials **14**, 1008 (2015).
- ⁸ C. Ye, W. Ruan, P. Cai, X. Li, A. Wang, X. Chen, and Y. Wang, Phys. Rev. X **5**, 021013 (2015).
- ⁹ Q. Si and E. Abrahams, Phys. Rev. Lett. **101**, 076401 (2008).
- ¹⁰ C.-H. Wang, C. M. Ainsworth, S. D. Champion, G. A. Stewart, M. C. Worsdale, T. Lancaster, S. J. Blundell, H. E. A. Brand, and J. S. O. Evans Phys. Rev. Materials **1**, 034403 (2017).
- ¹¹ N. Ni, S. Jia, Q. Huang, E. Climent-Pascual, and R. J. Cava, Phys. Rev. B **83**, 224403 (2011).
- ¹² J. B. He, D. M. Wang, H. L. Shi, H. X. Yang, J. Q. Li, and G. F. Chen, Phys. Rev. B **84**, 205212 (2011).
- ¹³ H. Zhang, X. Wu, D. Li, S. Jin, X. Chen, T. Zhang, Z. Lin, S. Shen, D. Yuan, and X. Chen, J. Phys.: Condens. Matter **28**, 145701 (2016).
- ¹⁴ J.-X. Zhu, R. Yu, H. Wang, L. L. Zhao, M. D. Jones, J. Dai, E. Abrahams, E. Morosan, M. Fang, and Q. Si, Phys. Rev. Lett. **104**, 216405 (2010).
- ¹⁵ M. Imada, A. Fujimori, and Y. Tokura, Rev. Mod. Phys. **70**, 1039 (1998).
- ¹⁶ Z.G. Chen, R.H. Yuan, T. Dong, G. Xu, Y.G. Shi, P. Zheng, J.L. Luo, J.G. Guo, X.L. Chen, and N.L. Wang, Phys. Rev. B **83**, 220507(R) (2011); F. Chen, M. Xu, Q.Q. Ge, Y. Zhang, Z.R. Ye, L.X. Yang, J. Jiang, B.P. Xie, R.C. Che, M. Zhang, A.F. Wang, X.H. Chen, D.W. Shen, X.M. Xie, M.H. Jiang, J.P. Hu, and D.L. Feng, Phys. Rev. X **1**, 021020 (2011).
- ¹⁷ P. Phillips, T.-P. Choy, and R.G. Leigh, Rep. Prog. Phys. **72**, 036501 (2009).
- ¹⁸ H. Kabbour, E. Janod, B. Corraze, M. Danot, C. Lee, M.-H. Whangbo, and L. Cario, J. Am. Chem. Soc. **130**, 8261 (2008).
- ¹⁹ F. Han, X. Wan, B. Shen, and H.-H. Wen, Physical Review B **86**, 014411 (2012).
- ²⁰ G. Baskaran, J. Phys. Soc. Jpn. **77**, 113713 (2008); R. Yu, J.-X. Zhu, and Q. Si, Phys. Rev. Lett. **106**, 186401 (2011).
- ²¹ Q. Si, Nature Phys. **5**, 629 (2009); M.M. Qazilbash, J.J. Hamlin, R.E. Baumbach, L. Zhang, D.J. Singh, M.B. Maple, D.N. Basov, Nature Phys. **5**, 647 (2009).
- ²² L. Craco, M.S. Laad, and S. Leoni, J. Phys.: Condens. Matter. **26**, 145602 (2014).
- ²³ B. Freelon, Y. H. Liu, J.-L. Chen, L. Craco, M. S. Laad, S. Leoni, J. Chen, L. Tao, H. Wang, R. Flauca, Z. Yamani, M. Fang, C. Chang, J.-H. Guo, and Z. Hussain, Phys. Rev. B **92**, 155139 (2015).
- ²⁴ G. Kotliar, S.Y. Savrasov, K. Haule, V.S. Oudovenko, O. Parcollet, and C.A. Marianetti, Rev. Mod. Phys. **78**, 865, (2006).
- ²⁵ T.-P. Choy and P. Phillips, Phys. Rev. Lett. **95**, 196405 (2005).
- ²⁶ G. S. Boebinger, Y. Ando, A. Passner, T. Kimura, M. Okuya, J. Shimoyama, K. Kishio, K. Tamasaku, N. Ichikawa, and S. Uchida, Phys. Rev. Lett. **77**, 5417 (1996); K. Semba and A. Matsuda, Phys. Rev. Lett. **86**, 496 (2001).
- ²⁷ J.W. Simonson, K. Post, C. Marques, G. Smith, O. Khatib, D.N. Basov, and M.C. Aronson, Phys. Rev. B **84**, 165129 (2011); Y. Shiomi, S. Ishiwata, Y. Taguchi, and Y. Tokura, Phys. Rev. B **84**, 054519 (2011).
- ²⁸ See, for example, J. M. Ok, S.-H. Baek, D. V. Efremov, R. Kappenberger, S. Aswartham, J. S. Kim, J. van den Brink, B. Büchner, arXiv:1802.09980, and references therein.
- ²⁹ O.K. Andersen, Phys. Rev. B **12**, 3060 (1975).
- ³⁰ V. Antonov, B. Harmon, and A. Yaresko, *Electronic structure and magneto-optical properties of solids* (Kluwer Academic Publishers, Dordrecht, Boston, London, 2004).
- ³¹ J. P. Perdew and Y. Wang, Phys. Rev. B **45**, 13244 (1992).
- ³² G. Giovannetti, L. de' Medici, M. Aichhorn, and M. Capone, Phys. Rev. B **91**, 085124 (2015)
- ³³ L. de' Medici, J. Mravlje, and A. Georges, Phys. Rev. Lett. **107**, 256401 (2011).
- ³⁴ B. Freelon, R. Sarkar, S. Kamusella, F. Brückner, V. Grinenko, S. Acharya, M. S. Laad, L. Craco, Z. Yamani, R. Flacau, I. Swainson, Y. Liu, H. Wang, J. Du, M. Fang, and H.-H. Klauss, arXiv:1708.01693.
- ³⁵ See, for example, L. Craco, M. S. Laad, S. Leoni, and H. Rosner, Phys. Rev. B **78**, 134511 (2008); L. Craco and S. Leoni, Scientific Reports **7**, 46439 (2017).
- ³⁶ L. Craco, Phys. Rev. B **77**, 125122 (2008).
- ³⁷ See also, C. Pépin, Phys. Rev. B **77**, 245129 (2008); M. Neupane, P. Richard, Z.-H. Pan, Y.-M. Xu, R. Jin, D. Mandrus, X. Dai, Z. Fang, Z. Wang, and H. Ding, Phys. Rev. Lett. **103**, 097001 (2009); R. Yu and Q. Si, Phys. Rev. Lett. **110**, 146402 (2013); Z.-Y. Song, H. Lee, and Y.-Z. Zhang, New J. Phys. **17**, 033034 (2015).
- ³⁸ L. de Medici, G. Giovannetti, and M. Capone, Phys. Rev. Lett. **112**, 177001 (2014).
- ³⁹ C. M. Varma, Z. Nussinov, W. van Saarloos, Physics Reports **361**, 267 (2002); see also, N. Trivedi, Nature Phys. **4**, 163 (2008) and references therein.
- ⁴⁰ L. Craco and M. S. Laad, Phys. Rev. B **80**, 054520 (2009).
- ⁴¹ R. Žitko, Ž. Osolin, and P. Jeglić, Phys. Rev. B **91**, 155111 (2015).
- ⁴² N. Dasari, N. S. Vidhyadhiraja, M. Jarrell, and R. H. McKenzie Phys. Rev. B **95**, 165105 (2017).
- ⁴³ T. Goto, S. Nakajima, M. Kikuchi, Y. Syono, and T. Fukase, Phys. Rev. B **54**, 3562 (1996).
- ⁴⁴ S. Mandal, P. Zhang, S. Ismail-Beigi, and K. Haule, Phys. Rev. Lett. **119**, 067004 (2017).